Sixth International Conference on Durability of Concrete Structures **Paper Number DSM10**
18 - 20 July 2018
University of Leeds, Leeds, West Yorkshire, LS2 9JT, United Kingdom

FEM Analysis of Structural Behaviour of Reinforced Concrete Beam under the Effect of Frost Damage

Z. Wang and T. Ueda
Laboratory of Engineering for Maintenance System, Faculty of Engineering, Hokkaido University, Japan

H. Hayashida
Civil Engineering Research Institute for Cold Region, Japan

D. Zhang
College of Civil Engineering and Architecture, Zhejiang University, China

ABSTRACT

Minimizing frost damage is one of the important durability issues for concrete structures in cold and wet areas. This paper performed a Finite Element Model (FEM) analysis on the structural behavior of reinforced concrete beam under the effect of frost damage. The frost damage was considered as degradations in two constituents: concrete material and bond between concrete and reinforcement. The constitutive models of deteriorated concrete material were proposed using a mesoscale simulation approach (Rigid Body Spring Model). DIANA FEA program was adopted for the structural analysis and experiments were also conducted for the verification. It was clarified that the structural performance of reinforced concrete beam under frost damage could be well evaluated by the FEM analysis. The assessment of the structural behavior of concrete members with frost damage would be achieved with this method.

Keywords: reinforced concrete, structural performance, frost damage, finite element model

1.0 INTRODUCTION

Frost action has detrimental effects on concrete structures in cold and wet regions which would lead the structures faster to deteriorate and thus shorten their lifetime. Demands for evaluating and predicting the degradation of concrete structure under frost damage are growing to acquire the optimized maintenance and reparation.

Many studies have been conducted on the mechanism of frost damage in porous materials and modeling of the frost damaged materials. Gong *et al.* (2015a) developed a comprehensive internal pressure model which could explain the different experimental observations that porous materials showed both expansion and contraction during the freezing and thawing cycles. Based on the Rigid Body Spring Model developed by Nagai *et al.* (2004) and modified material constitutive relationship with considering the degradation by Ueda *et al.* (2009), mesoscopic simulation of mechanical behaviors of concrete under frost damage has been successfully achieved (Gong *et al.* 2015b). With this simulation program, numerical analysis and modeling of compressive and tensile behaviors of concrete suffering FTCs were conducted by Wang *et al.* (2017).

While most previous researches have been concerned with the degradation of concrete materials in freezing-thawing environment, relatively little attention has been focused on the members' behaviors such as beam, column etc. under the effect of frost action. With the deteriorated material constitutive models proposed by the authors (Wang *et al.* 2017), this paper has been devoted to the FEM analysis of structural performance under the effect of frost damage. Firstly, the degradation models proposed via mesoscopic simulation program were briefly introduced. Second, the two-dimensional FEM analysis was conducted by applying the proposed material models into simulation. Finally, experimental work was carried to investigate the simulation results where satisfactory agreement was found, which strongly demonstrated the applicability of this approach to evaluate the structural behavior of RC beam under effect of frost damage.

2.0 MODELING OF THE FROST DAMAGED MATERIAL BEHAVIORS WITH RBSM

2.1 RBSM Frost Damage Analysis Program

Rigid Body Spring Model (RBSM) is a discrete numerical analysis method which is proper to

simulate splitting and cracking issues and suitable for static and small deformation problems (Nagai *et al.* 2004). The model in RBSM is composed of polyhedron elements which are representing for mortar and aggregate cells and connected by normal and shear springs. Each element has two transitional and one rotational degree of freedom at the centre of elemental gravity, as shown in Fig. 1. Considering that mortar is not homogeneous material, a normal distribution is simply assumed for the tensile strength of normal springs, see Eq. (1).

$$f\left(f_{t,elem}\right)=\frac{\exp\left[\left(f_{t,elem}-\mu\right)^2/2s^2\right]}{\sqrt{2\pi}s} \qquad (1)$$
$$s=-0.2\mu+1.5$$

where $f_{t,elem}$ [MPa] is the tensile strength of the element and for $f_{t,elem}$<0, assuming $f_{t,elem}$=0; μ [MPa] is the average value of $f_{t,elem}$ and s [MPa] is the standard derivation.

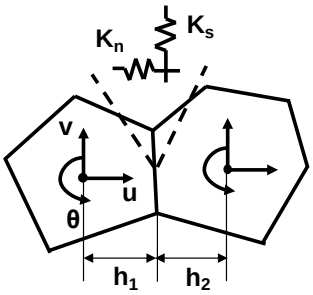

K_n K_s: Stiffness of normal and shear springs
u v θ : Degree of freedom for Voronoi elements

Fig. 1. Schematic of elements, springs and DOFs

For porous materials suffering from frost damage, the stress-strain relationship for normal springs was modified to consider the unrecoverable plastic deformation (Ueda *et al.* 2009). The unloading and reloading path would follow the envelope curve with slope k_1' (the dash line) instead of k_1 (the solid line) once the maximum historical strain is larger than ε_0, see Fig. 2.

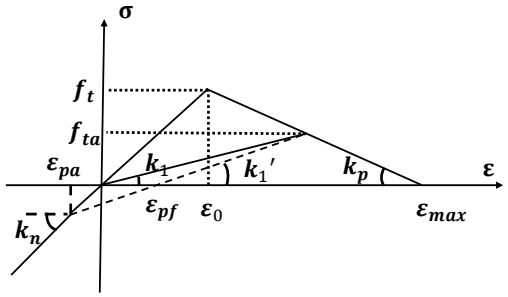

Fig. 2. Stress-strain relationships for tensile springs

Some theories have been developed to explain the internal pressure during the ice formation and Gong *et al.* (2015a) proposed a mathematical model considering three types of force: hydraulic pressure, crystallization pressure and cryosuction pressure, see Eq. (2). In this model, the total pressure by ice formation could be positive (expansive) or negative (contractive) depending on the environmental conditions such as temperature, saturation degree, etc. Mesoscale simulation was also conducted where satisfactory agreement was found between experiment and simulation results to support the applicability of this simulation program (Gong *et al.* 2015b).

$$0.09\phi\dot{\psi}_c-\frac{A}{V}\cdot\frac{m}{\eta}\cdot\frac{2}{R_E-r_E}P_h=\left(\frac{b}{K_p}+\frac{\phi\psi_i}{K_i}+\frac{\phi\psi_l}{K_l}\right)\cdot\dot{P}_h$$
$$P_l=\psi_l\cdot\Delta S_{fv}\cdot\left(T-T_0\right) \qquad (2)$$
$$P_c=-\psi_l\cdot\left(1-\gamma\right)\cdot\Delta S_{fv}\cdot\left(T-T_0\right)$$

where p_h, p_l and p_c [MPa] represent the hydraulic pressure, cryosuction pressure and crystallization pressure, respectively.

Based on the mesoscale simulation program, numerical analysis and parametric studies were conducted by the authors to model the macroscale mechanical behaviours of concrete under effect of frost damage (Wang *et al.* 2017), which will be stated in the following section. The degradation in both compression and tension of concrete were predicted on basis of the simulation results.

2.2 Modelling of Mechanical Behaviours of Damaged Concrete with RBSM Program

Considering the most adopted cases in laboratories and engineering applications, concrete specimens with water cement ratio equalling to 0.4, 0.5 and 0.6 were simulated under different temperatures (0, -10, -15, -20, -30 and -40 ºC) and FTC numbers (0, 50, 100, 150, 200 and 300). All the models had same dimension of 100x200 mm^2 where volume fraction of aggregate was set to be 40%. Voronoi polyhedron elements were automatically meshed and the element size was around 3 mm. The specimens were tested with compressive and splitting tensile loading after suffering the freezing and thawing cycles. Material inputs such as strength of the springs, factors in failure criterion, void ratio of concrete etc. were set according to the value suggested by Nagai *et al.* 2004 and Gong *et al.* 2016, see Table 1. In Table 1, f'_{cm} [MPa] and E_m [MPa] is the compressive strength and elastic modulus of mortar; f_{tp} [MPa] is the pure tensile strength of mortar; f_{ti} [MPa] is the tensile strength of ITZ; *w/c* is the water cement ratio and *c* is the parameter in interface criterion; φ_i is the void ratio.

Table 1. Material inputs for concrete specimens

w/c	f_{cm} (MPa)	E_m (MPa)	f_{tp} (MPa)	f_{ti} (MPa)	*c* (MPa)	φ_i
0.4	42.55	23400	3.75	1.72	2.86	0.18
0.5	31.91	21200	3.35	1.58	2.60	0.22
0.6	24.84	19200	3.00	1.44	2.34	0.26

Results of compressive and splitting tensile tests of frost damaged concrete were analysed and the material models were proposed based on the prediction of relative compressive strength R_{fc}, which was the ratio between compressive strength of frost damaged concrete and that of non-damaged concrete. By regression from simulation data, the deteriorated compressive strength could be predicted as Eq. (3).

$$\begin{aligned} &R_{f_c} = 1 - N(a \ln(-T_{\min}) + b) \\ &\begin{cases} a = 0.0015 w/c + 0.0006 \\ b = -0.006 w/c + 0.0051 \end{cases} \end{aligned} \tag{3}$$

where T_{min} is the minimum temperature in each FTC; a and b are fitting parameters considering water cement ratio (w/c); N is the number of FT cycles.

The predicted compressive strength was also compared with some experiment evidences where good correlations have been found to support the prediction model (Eq. (3)), as shown in Fig. 3. Besides compressive strength, the elastic modulus, strain at compressive peak stress and tensile strength of frost damaged concrete were also modelled based on the value of R_{fc}, see Eq. (4).

$$\begin{aligned} &R_{E_c} = 1.284^{2.932 R_{f_c}} - 1.081 \\ &R_{\varepsilon_c} = -1.261 R_{f_c} + 2.261 \\ &R_{f_t} = 0.89 \exp[3.13 \times (R_{f_c} - 1)] + 0.11 \end{aligned} \tag{4}$$

where R_{Ec}, $R_{\varepsilon c}$ *and* R_{ft} stand for the relative elastic modulus, relative strain at compressive peak stress and relative tensile strength between frost damaged concrete and non-damaged concrete. The proposed models were also verified to be reliable and applicable by various previous experimental data (Wang *et al.* 2017).

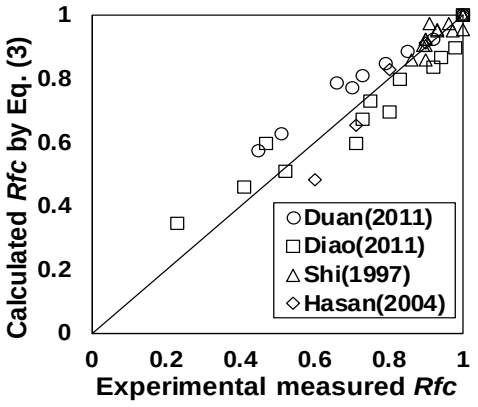

Fig. 3. Comparison of R_{fc} between calculated results and experimental data

For the compressive stress-strain relationship, the constitutive model for non-damaged concrete proposed by Guo *et al.* (2003) was adopted since it could describe the "stiffness recovery" effect for frost damaged concrete by two shape controlling parameters a (for ascending branch) and b (for descending branch), as shown in Eq. (5). Previous experimental data was used to model the shape controlling parameters by relating R_a and R_b with relative compressive strength R_{fc}, see Eq. (6) (Wang *et al.* 2017).

$$\frac{\sigma}{f_c} = \begin{cases} a\varepsilon / \varepsilon_c + (3-2a)(\varepsilon / \varepsilon_c)^2 + (a-2)(\varepsilon / \varepsilon_c)^3 \\ \dfrac{\varepsilon / \varepsilon_c}{b(\varepsilon / \varepsilon_c - 1)^2 + \varepsilon / \varepsilon_c} \end{cases} \tag{5}$$

$$\begin{aligned} &R_a = 0.833 R_{f_c}^{3.512} + 0.167 \\ &R_b = -1.507 R_{f_c}^{2.715} + 2.507 \end{aligned} \tag{6}$$

where R_a *and* R_b are the ratio calculated as a_d/a and b_d/b, where subscript stands for frost damaged case.

For tensile stress-strain relationship, bilinear model was adopted for the post-peak constitutive law (Eq. (7)) and the turning point was suggested depending on the experimental results by Hanjari *et al.* (2011). Besides, the maximum crack width for frost damaged concrete was provided based on the available test results (Hasan *et al.* 2002, Hanjari *et al.* 2011), see Eq. (8).

$$\begin{aligned} &\sigma / f_{td} = 1 - 5.929 w / w_{d\max} \quad (w / w_{d\max} \le 0.14) \\ &\sigma / f_{td} = 0.198(1 - w / w_{d\max}) \quad (w / w_{d\max} > 0.14) \end{aligned} \tag{7}$$

$$R_{w\max} = 6.716 e^{-1.821 R_{ft}} \tag{8}$$

The proposed compressive and tensile constitutive models were both verified by various experimental results (see Fig. 4 and Fig. 5 (Wang *et al.* 2017)).

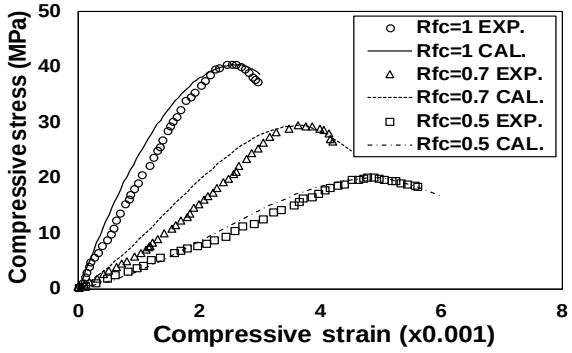

Fig. 4. Comparison of compressive curve between proposed model and test results (Hanjari *et al.* 2011)

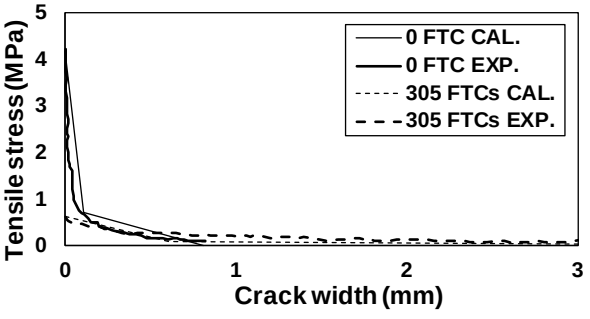

Fig. 5. Comparison of post tensile curve between proposed model and test results (Hasan *et al.* 2002)

3.0 FEM ANALYSIS OF RC BEAM BEHAVIOR WITH PROPOSED MATERIAL MODELS

3.1 Material Behaviours Based on Proposed Models

The material properties adopted in FEM analysis were determined as the measurement in verification test which would be introduced in next chapter. The compressive strength of the sound (non-frost damaged) concrete was given as 22.7 MPa. Measurement of elastic modulus, tensile strength and compressive peak strain were not conducted but such values could be easily calculated based on some recommendations. For instance, the elastic modulus and tensile strength could be calculated according to JSCE Standard Specifications for Concrete Structures, and the compressive peak strain could be calculated as the suggestion by Nicolo *et al.* (1994). In this study, these values were calculated based on Eq. (9) according to the given compressive strength and the results were all listed in Table 2. For compressive constitutive law of sound concrete, shape controlling parameters *a* and *b* could be adopted based on compressive strength as suggested by Guo *et al.* (2003), see Table 2. For post tensile constitutive law of non-damaged concrete, the maximum crack width was adopted to be 0.08 mm.

$$E = \left(2.2 + \frac{f_c - 18}{20}\right) \times 10^4$$
$$f_t = 0.23\left(f_c\right)^{2/3} \quad (9)$$
$$\varepsilon_c = 1.491 \times 10^{-5} f_c + 0.00195$$

where f_c, f_t, ε_c and E stand for the compressive strength, tensile strength, compressive peak strain and Elastic modulus for sound concrete.

Table 2. Material characteristics for concrete

Type	f_c (MPa)	E (MPa)	f_t (MPa)	ε_c (x10^{-6})	*a*	*b*
Sound	22.70	24350	1.84	2288	2.10	0.99
Damaged	13.12	10873	0.64	3506	0.61	2.15

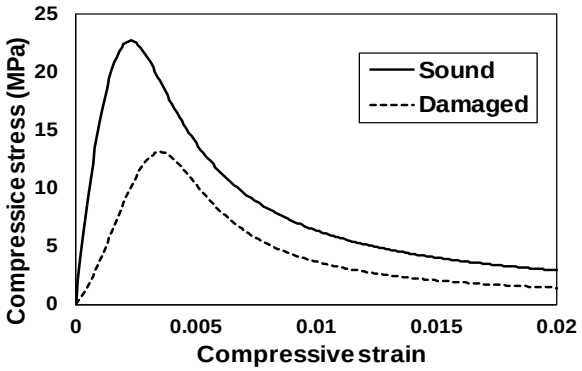

Fig. 6. Compressive constitutive law for sound and frost damaged concrete

For frost damaged concrete, the compressive strength was set to be 13.12 MPa, where in the verification experiment this value was also achieved. Thus, the elastic modulus, compressive peak strain and tensile strength for frost damaged concrete could be given according to the proposed models, see Eq. (4). Besides, the shape controlling parameters a_d and b_d could be calculated as Eq. (6) and all the values were listed in Table 2. Based on Eq. (8), the maximum crack width for frost damaged concrete was calculated to be 0.28 mm.

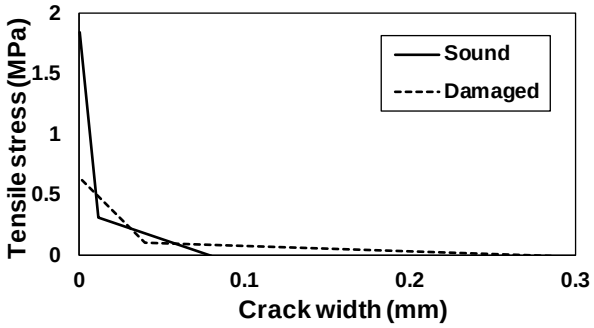

Fig. 7. Post tensile constitutive law for sound and frost damaged concrete

The compressive and post tensile constitutive relationships for both sound and damaged concrete were drawn according to the above statements, see Figs. 6 and 7.

3.2 Finite Element Model Analysis with DIANA

The structural performance of both sound and frost damaged RC beam (naming “N” and “F” in the following statement) was analysed with 2D finite element model using DIANA FEA program (version 10.1).

Modelling of Concrete

Four node quadrilateral plane stress solid element was adopted for concrete. To simulate the cracking behaviour of concrete, rotating smeared crack model was used so that the non-linear compressive behaviour could be taken into consideration (Rots *et al.* 1989). Crack band width was manually set to be same as the element size (40 mm) to have a good approximation of the localisation zone as suggested by Hanjari *et al.* (2013).

Since localisation of deformations in compressive failure should be considered, the compressive stress-strain relationship in the numerical analysis (Fig. (6)) needed to be calibrated where the compressive softening curve should be modified according to the element size in RBSM simulation and finite element models (Hanjari *et al.* 2013). As a result, considering the model in RBSM simulation was 100x200 mm^2 (Wang *et al.* 2017) and the element size in DIANA FEA was 40x40 mm^2, the compressive softening curve was modified as Fig. 8.

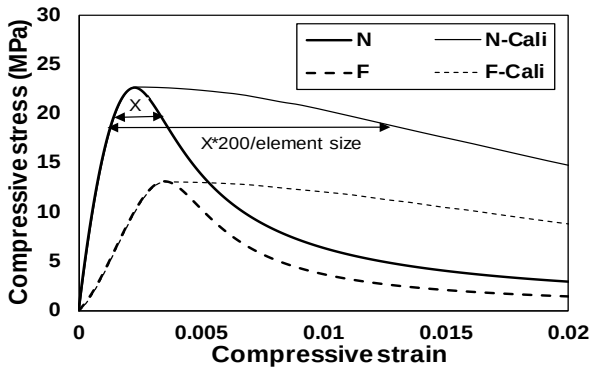

Fig. 8. Calibration of the compressive stress-strain curve according to element size in FEM analysis

Modelling of Reinforcement and Interface

For modelling the rebars, the truss reinforcement element was adopted with stiffness E_s of 200 GPa and yielding strength σ_y of 370 MPa. After yielding, secondary hardening was considered with stiffness E_s' of 2000 MPa ($0.01E_s$) (see Fig. 9). All the values were achieved as well in the verification experiment which will be stated in the following chapter. The reinforcement was embedded in the concrete element, in other words, no bond-slip relationship was considered in the current FEM simulation.

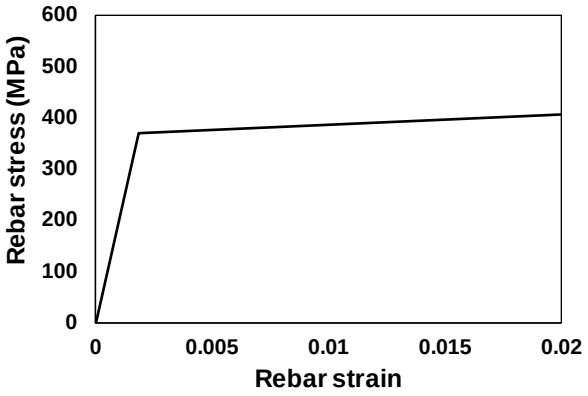

Fig. 9. Stress-strain relationship for rebar in FEM

Modelling of RC Beam

The RC beam was modelled after the materials properties were confirmed as stated in the above sections. The cross-section of the beam model was 200x200 mm^2 and span length was 1200 mm. Loading plate and supporting plates were added with steel properties and dimension of 10x80 mm^2 to avoid the stress concentration around the loading point and supporting points. Point loading controlled by displacement of 0.1 mm per interval was given at centre point of the loading plate. Pinned support and roller support were set at the centre point of each supporting plate respectively. Afterwards, 40x40 mm^2 quad-mesh was generated, as shown in Fig. 10. Newton-Raphson iteration method was adopted during the calculation.

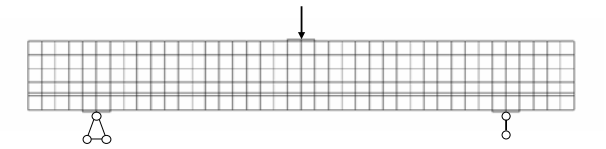

Fig. 10. Schematic of RC beam model in DIANA

4.0 EXPERIMENT VERIFICATION

Experiment of static loading on sound reinforced concrete beam and frost damaged reinforced concrete beam was conducted as the verification to the FEM analysis.

4.1 Specimen Preparation

Two beams (naming “N” and “F”, which represented for the non-damaged beam and the frost damaged beam respectively) were prepared with cross-sectional dimension of 200x200 mm^2 and span length of 1200 mm (see Fig. 11). Concrete was made with Ordinary Portland Cement and coarse aggregate was crushed stone with a maximum grain size of 20 mm. To achieve an accelerated degradation from FTC, the water cement ratio was chosen to be 0.65 and the compressive strength of concrete at 28 days was 22.7 MPa. For each beam, two reinforcement bars with diameter of 13 mm and yielding strength of 370 MPa were embedded. Strain gages were attached to the reinforcements at interval of 200 mm, see Fig. 11.

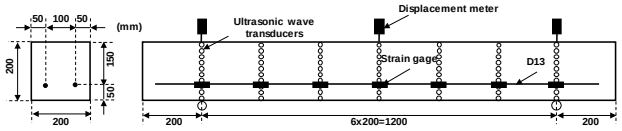

Fig. 11. Configuration of reinforced concrete beam

4.2 FTC and Loading

For beam “F”, freezing and thawing cycles was adopted as ASTM C666-B method, where the specimen was frozen in air and thawed in water. The RC beam was set in a large container with water filled and drained automatically by the controlling system. The whole setup was put into the FTC chamber which had the cooling and heating appliance. During the thawing process, water will be poured into the container to achieve the water thawing condition and ensure the saturation degree and it will be drained out before freezing process started to achieve the air freezing condition.

To achieve the objective compressive strength for concrete (13.12 MPa), the frost damage procedure was controlled by ultrasonic wave propagation velocity measurement: the authors have once proposed a relationship between the compressive strength and ultrasonic wave transmitting velocity

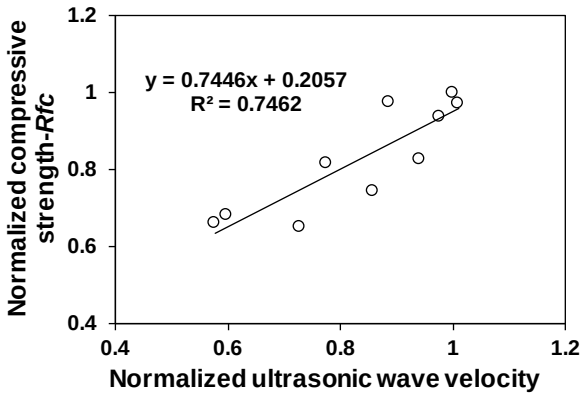

Fig. 12. Relationship between ultrasonic transmitting velocity and compressive strength of concrete

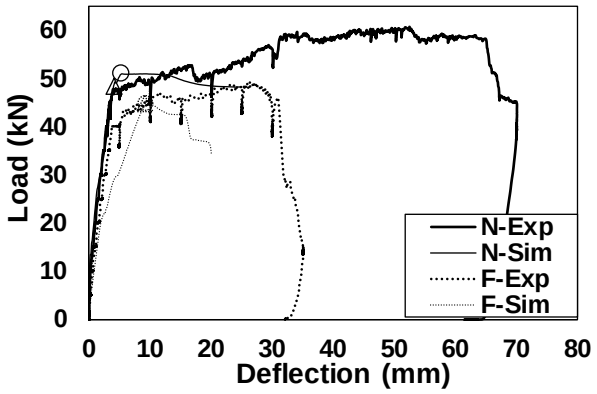

Fig. 13. Load-displacement curves of beam N and F by experiment and FEM simulation

(Hayashida *et al.* 2014), as Fig. 12. It was calculated that the compressive strength of concrete could decrease from 22.7 MPa to 13.12 MPa if the ultrasonic wave transmitting velocity decreased into 50% of its original value.

In the test, each FTC had a minimum temperature of -18 ºC and maximum temperature of +5 ºC and FTC stopped at 308th cycle, where the ultrasonic wave propagation velocity decreased from 4 km/s to 2 km/s. Ultrasonic wave transducers (D20) were arranged with 20 mm interval in vertical direction at the opposite sides of cross sections where strain gages were attached, as shown in Fig. 12. A frequency of 28 kHz and voltage of 1 kV ultrasonic wave was adopted in the test.

After the frost damage level was reached for specimen “F”, static 3-point bending test was applied for both specimens “N” and “F”. Displacement meters were placed at the supporting and loading point (see Fig. 11). Load, displacement and strain of the reinforcement were measured during the test.

4.3 Results and Discussion

Load-Displacement Relationships

Fig. 13 shows the load-displacement curves of beam “N” and “F” by both experiment and FEM simulation. Sections of the load-displacement curves where displacement between 0 mm and 20 mm were also drawn as shown in Fig. 14.

From the figures, it could be found that for the RC beam without frost damage, the simulation could predict the pre-yielding range well. The load and displacement of beam “N” when reinforcement yielded (naming yielding load in the following content) measured in the test was 47.3 kN and 4 mm, respectively. In the simulation, the values were 49.3 kN and 4.2 mm where the simulation showed slightly larger values in yielding loading and displacement. For post-yielding range of beam “N", simulation showed that the maximum load (50.9 kN) was reached at displacement of 5.4 mm, which was soon after the rebar yielded. While in the

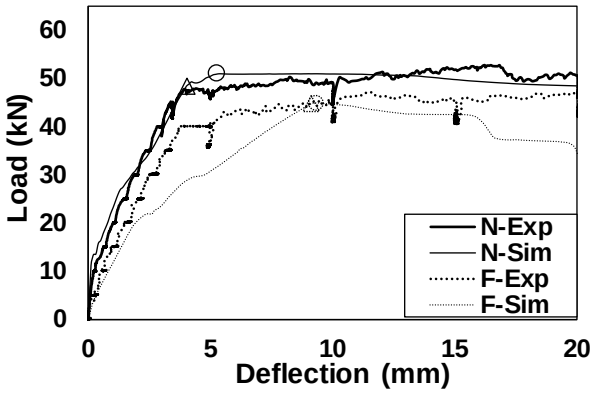

Fig. 14. Load-displacement curves of beam N and F with displacement between 0-20 mm

experiment, load kept increasing slowly after rebar yielded until it reached the maximum load (61 kN) at deformation of 52 mm.

For the frost damaged beam “F”, simulation results showed an obvious smaller stiffness than the test results before yielding of the rebar. In FEM analysis, the yielding happened when displacement reached 9.2 mm with yielding load of 44.8 kN. While in the test, yielding of rebar took place when displacement only reached 4 mm and the yielding load was 40.1 kN. The reason of such difference was considered that the real frost damage condition in the test was not uniform. Though the ultrasonic wave velocity has decreased into 50% in the parallel measurement (Fig. 11), the value only represented the average damage along the wave transmitting path. Due to the thermal lag and moisture transfer effect, surface area would always have a more severe damage than the inner area (Wang *et al.* 2017), which could not be reflected in the current 2D analysis. As a result, 3D analysis is in strongly needed together with the examination of the damage distribution. Post-yielding behaviours of beam “F” showed uncorrelations between simulation and experiment, where the analysis showed a quick decreasing of load once the yielding load was reached while the test indicated a slow increasing of load before the

maximum loading capacity was reached (49.41 kN) at displacement of 26 mm.

From the comparison, it is indicated that the pre-yielding performance of both sound and frost damaged beam could be simulated through the proposed materials models and FEM analytical approach. For beam “N” at yielding load in the simulation, concrete almost reached its compressive peak strain, which means that the compressive strength was close and concrete would soon turn into the softening branch. As a result, the maximum load was achieved soon after the yielding and load started to decrease. Different observation was found in the test for beam “N” that after yielding, concrete could still be able to sustain compressive stress until the deformation was very large. The reason was considered that the roller support in the test could offer additional restriction in horizontal direction when it was intermittently stuck by friction. Due to such additional effect, concrete in compression zone could sustain higher stress and thus the load could increase. But such effect would be released when the roller moved again and as a result, the load would decrease again. It could be proved by Fig. 13 where the load of “N-Exp” showed increasing-deceasing frequently after the yielding load. For the similar reason, the beam “F” also showed slightly load increasing in the test while decreasing in the FEM analysis.

Cracking Propagation at Yielding Load

Besides the load-displacement curves, cracking figures when rebar yielded were also drawn from experiment and FEM analysis, see Figs. 15 and 16 for beam “N” and “F”, respectively. In the figures, black lines stand for observations from experiment.

For beam “N”, several flexural cracks appeared in the region between -50 cm to 30 cm from the centre in the test, which was successfully simulated by the FEM analysis. In both simulation and experiment, it was found that cracks at yielding load near the midpoint were so long as to reach the upper surface of the beam. For beam “F”, it was observed in the test that cracks were shorter than that for beam “N” at yielding load, which was also simulated in the analysis.

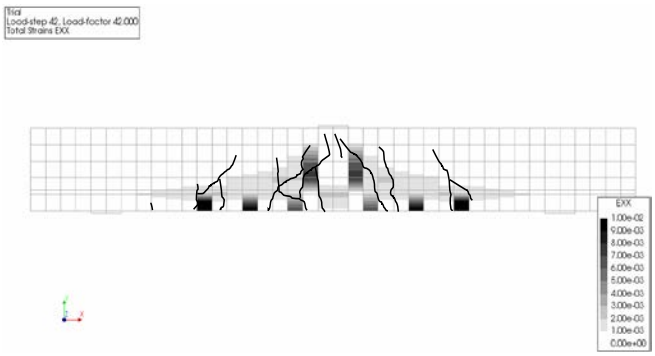

Fig. 15. Cracking illustration of beam N at yielding load by experiment and FEM analysis

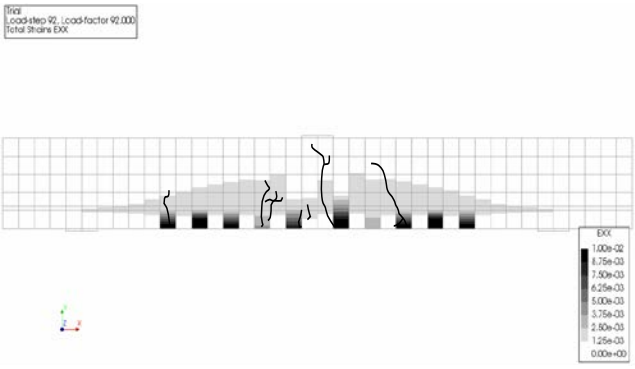

Fig. 16. Cracking illustration of beam F at yielding load by experiment and FEM analysis

5.0 CONCLUSIONS

1. In this paper, the two-dimensional (2D) FEM analysis on the flexural behaviours of reinforced beam under frost damage was conducted by applying the deteriorated constitutive models proposed from mesoscale Rigid Body Spring Model program. Verification experiment was also carried to investigate the reliability of the approach, where reasonable results were found which indicates that the approach is applicable to evaluate the flexural behaviour of RC beam under frost damage. The pre-yielding behaviours (load-displacement curve, cracking propagation) tended to be predicted well by FEM analysis while the post-yielding behaviours showed some uncorrelations between FEM and experiment.

2. In the current work, the bond-slip relationship between concrete and rebar under FTCs was not taken into consideration since a generally-accepted degradation law for bond-slip has not been established yet. As a future study, the mesoscale program focusing on the bond-slip properties under frost damage would be developed based on Rigid Body Spring Model. Accordingly, a three-dimensional (3D) FEM analysis would be conducted with considering the degradation in both concrete materials and bond-slip relationship.

Acknowledgement

The authors would like to express great thanks to the Grand-in-Aid for Scientific Research (A) of Japan Society of Promotion of Science (No. 26249064) and the scholarship from Japan Ministry of Education, Culture, Sports and Technology (MEXT).

References

De Nicolo, B., Pani, L. and Pozzo, E., 1994. Strain of concrete at peak compressive stress for a wide range of compressive strengths. Materials and Structures, 27(4):206-210.

Gong, F., Sicat, E., Zhang, D. and Ueda, T., 2015a. Stress analysis for concrete materials under multiple freeze-thaw cycles. Journal of Advanced Concrete Technology, 13(3):124-134.

Gong, F., Wang, Y., Zhang, D. and Ueda, T., 2015b. Mesoscale simulation of deformation for mortar and concrete under cyclic freezing and thawing stress. Journal of Advanced Concrete Technology, 13(6):291-304.

Guo, Z. and Shi, X., 2003. Reinforced concrete theory and analysis, Tsinghua University Press, Beijing, China.

Hanjari, K.Z., Kettil, P. and Lundgren, K., 2013. Modelling the structural behaviour of frost-damaged reinforced concrete structures. Structural and Infrastructure Engineering, 9(5):416-431.

Hanjari, K.Z., Utgenannt, P. and Lundgren, K., 2011. Experimental Study of the material and bond properties of frost-damaged concrete. Cement and Concrete Research, 41(3):244-254.

Hayashida, H., Sato, Y. and Ueda, T., 2014. Structural property evaluation of freeze-thaw-damaged RC beam members by nonlinear finite element analysis. The 4th International Conference on the Durability of Concrete Structures, West Lafayette, USA.

Nagai, K., Sato, Y. and Ueda, T., 2004. Mesoscale simulation of failure of mortar and concrete by 2D RBSM. Journal of Advanced Concrete Technology, 2(3):359-374.

Rots, J.G. and Blaauwendraad, J., 1989. Crack models for concrete, discrete or smeared? Fixed, multi-directional or rotating?. HERON, 34(1).

Ueda, T., Hasan, M., Nagai, K., Sato, Y. and Wang, L., 2009. Mesoscale simulation of influence of frost damage on mechanical properties of concrete. Journal of Materials in Civil Engineering, 21(6):244-252.

Wang, Z., Zhang, D., Gong, F. and Ueda, T., 2017. Modeling of mechanical behaviour of concrete with frost damage based on 2D Rigid Body Spring Model. The 8th Aisa and Pacific Young Researchers and Graduates Symposium (YRGS2017), Tokyo, Japan.

Wang, Z., Gong, F., Zhang, D., Hayashida, H. and Ueda, T., 2017. Mesoscale simulation of concrete behaviour with non-uniform frost damage with verification by CT imaging. Construction and Building Materials, 157:203-213